Chemical Science

Accepted Manuscript

This article can be cited before page numbers have been issued, to do this please use: B. Li, M. Yuan, N. N. Xia, X. Hu and F. He, *Chem. Sci.*, 2025, DOI: 10.1039/D5SC05472A.

ROYAL SOCIETY OF CHEMISTRY

rsc.li/chemical-science

View Article Online
DOI: 10.1039/D5SC05472A

ARTICLE

Ligand-mediated asymmetric dicopper sites for robust catecholase-mimicking catalysis and selective sensing

Bojin Li,[a] Meng Yuan,[a] Nannan Xia,[b] Xun Hu*[a] and Fei He*[a]

Received 00th January 20xx,
Accepted 00th January 20xx

DOI: 10.1039/x0xx00000x

Fabricating dicopper centers in nanozymes offered a promising route to mimic catecholase-like catalysis. However, some dicopper centers often suffered from symmetric configurations, which was prone to weaken the O-O bond polarization, thereby limiting O_2 activation. This resulted in the unsatisfied intrinsic activities of nanozymes, thus hindering their potential sensing applications. Here, we reported a catechol oxidase (CO)-like nanozyme (DTD-Cu) engineered with proximally and asymmetrically coordinated dicopper centers via a N/S-rich ligand. The unique asymmetric N_4Cu-CuN_4S configuration facilitated the preferential O_2 adsorption/activation and the O-O bond polarization as well as subsequent 4-electron reduction to H_2O via a H_2O_2 intermediate, thus endowing DTD-Cu with dramatically enhanced intrinsic activity, as evidenced by orders-of-magnitude improvements in K_m and K_{cat}/K_m over most reported CO-like nanozymes and artificial enzymes. Capitalizing on this superior activity, we achieved highly selective and sensitive detection of the cytotoxic tris(2-carboxyethyl)phosphine (TCEP) with a detection limit of 98.6 ppb via a synergistic dual-inhibition mechanism involving both TCEP-induced reduction of the oxidized substrate/ROS and direct TCEP-dominated chelation to the Cu sites.

Introduction

Nanozymes, synthetic mimics of natural enzymes, offered compelling advantages such as high stability, cost-effectiveness, and tunable functionality, holding immense promise in replacing natural enzymes for various applications.[1-7] Among these, catechol oxidase (CO)-like nanozymes, which catalyzed the oxidation of catechol derivatives, are recently attractive for biomimetic catalysis and analytical sensing.[1, 4, 5, 8] However, a pervasive challenge of existing CO-like nanozymes was their relatively low catalytic activities, often reflected in poor Michaelis constant (K_m) and catalytic efficiency (K_{cat}/K_m) values,[1, 9-12] which curtailed their potential applications.

To boost the intrinsic activities of CO-like nanozymes, using ligand engineering to control the dicopper site configuration represented one of effective approaches,[13-16] which could mimic the dicopper centers of natural CO better[17, 18] compared with other strategies such as regulating multinuclear metal centers,[1, 12] changing the types of metal/support[9] and controlling metal-polymer or supramolecular self-assembly.[5, 19] Despite many progresses, some artificial dicopper centers often suffered from the weak O-O bond polarization due to their symmetric configurations (i.e., S_1N_3Cu-CuN_3S_1, S_1N_2Cu-CuN_2S_1, O_1N_3Cu-CuN_3O_1, O_3N_1Cu-CuN_1O_3),[4, 14, 15] which limited O_2 activation, thus resulting in the unsatisfied intrinsic activities. In this sense, breaking the symmetric configuration of dicopper sites through ligand engineering may be crucial for boosting the CO-mimicking activity of nanozyme, but remained a formidable task.

Here, we engineered a CO-like nanozyme (DTD-Cu) featuring proximally and asymmetrically coordinated dicopper catalytic centers by employing 2,5-diamino-1,3,4-thiadiazole (DTD) as a N/S-rich ligand. When applied for CO-mimicking catalysis, the dicopper sites with asymmetric N_4Cu-CuN_4S configuration promoted the O_2 adsorption and activation to generate reactive oxygen species and directed its rapid 4-electron reduction to H_2O, thereby enabling a dramatic enhancement in catalytic kinetic parameters, notably K_m and K_{cat}/K_m, by orders of magnitude compared to previously reported CO-like nanozymes and artificial enzymes. Leveraging this superior activity as well as the coordination capability of Cu for phosphorus, we demonstrated a highly selective colorimetric sensing platform for trace cytotoxic tris(2-carboxyethyl)phosphine (TCEP), where the detection limit approached 98.6ppb, lower than other sensing systems for detecting P-containing compounds based nanozymes, surface-enhanced Raman spectroscopy (SERS) and fluorescence.

Results and discussion

To construct adjacent dicopper centers, the heterocycle ligand (i.e., 2,5-diamino-1,3,4-thiadiazole, DTD) was chosen due to the existence of two neighbouring heterocyclic N atoms, which were capable of coordinating with Cu through a simple one-step complexation (see Experimental section in SI). Furthermore, the thiophenic S atom of DTD also possessed the

[a] School of Material Science and Engineering, University of Jinan, Jinan 250024, China, E-mail: xun.hu@outlook.com; mse_hef@ujn.edu.cn
[b] State Key Laboratory of Green Papermaking and Resource Recycling, Key Laboratory of Pulp & Paper Science and Technology of Shandong Province/Ministry of Education, Qilu University of Technology (Shandong Academy of Sciences), Jinan 250353, China

Supplementary Information available: [details of any supplementary information available should be included here]. See DOI: 10.1039/x0xx00000x

View Article Online
DOI: 10.1039/D5SC05472A

coordination potential for Cu, thus contributing to controlling the coordination configuration of Cu center in DTD-Cu (**Figure 1A**).

The microscopic morphology of DTD-Cu was observed using scanning electron microscope (SEM). DTD-Cu presented the bulk particle with the size of micron level (**Figure 1B**). When PVP was introduced into the preparation system, the size of DTD-Cu-PVP obviously decreased to the nanometer level compared with that of DTD-Cu (**Figure 1C**). The XRD patterns of DTD-Cu and DTD-Cu-PVP were nearly identical (**Figure S1**), indicating that adding PVP did not change the structure of DTD-Cu. According to the SEM image, the cross section of the DTD-Cu block particle presented the aggregated nanoparticle morphology, which could be demonstrated by the image of transmission electron microscope (TEM) (**Figure S2**). The similar morphology accompanied with the interconnected nanoparticles with an average size of ~26.5 nm was also found for DTD-Cu-PVP (**Figure 1D**). Energy dispersive spectroscopy (EDS) mapping showed that the elements of C, N, O, S and Cu uniformly distributed in DTD-Cu (**Figure 1E**). The Cu content in DTD-Cu was 23.3 wt.% based on ICP-OES analysis.

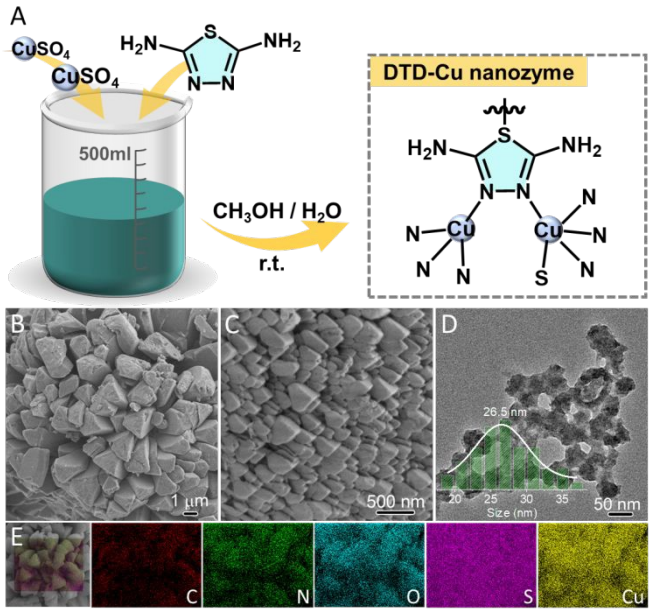

Figure 1 (A) Schematic illustration of synthesizing DTD-Cu nanozyme; SEM images of DTD-Cu prepared with (B) and without (C) PVP addition; (D) TEM image of DTD-Cu; (E) EDS mapping of DTD-Cu.

To explore the coordination information of Cu center, time-of-flight secondary ion mass spectrometry (TOF-SIMS) was carried out to collected the mass fragments knocked out from DTD-Cu.[20] The fragment ions with the mass to charge ratio (m/z) of 148.9 ($Cu_1C_2N_2S_1H_2$), 163.9 ($Cu_1C_2N_3S_1H_3$), 178.9 ($Cu_1C_2N_4S_1H_4$) and 294.9 ($Cu_1C_4N_8S_2H_8$) in the positive spectrum as well as 146.9 ($Cu_1C_2N_2S_1$) and 162.9 ($Cu_1C_2N_3S_1H_2$) in the negative spectrum were detected (**Figure 2A** and **2B**), respectively, which may correspond to Cu_1-coordinated DTD fragments involving the Cu-N and/or Cu-S coordination. The possible coordination between the heterocyclic N/S atoms of DTD and Cu was also supported by the appearance of Cu_2-coordinated DTD fragment ions with m/z of 225.8 ($Cu_2C_2N_3S_1H_2$) and 209.9 ($Cu_2C_2N_2S_1$).

X-ray photoelectron spectroscopy (XPS) was further conducted to determine the Cu-N/S coordination and chemical states of elements in DTD-Cu. According to XPS survey scan spectrum, C, N, O, S and Cu (**Figure S3**) were detected, consistent with the EDS mapping result. In the Cu2p spectrum, Cu^{2+} and Cu^{+} were observed (**Figure 2C**). The N1s spectrum displayed two signals, which were assigned to Cu-N and C-NH_2 with a ratio of ~1:1 (**Figure 2D**). This signified that Cu may coordinated with the heterocyclic nitrogen rather than exocyclic -NH_2, similar to the reported result.[14, 15] In the S2p spectrum, we observed three types of S, corresponding to SO_4^{2-}, C-S and Cu-S (**Figure 2E**). Fourier-transform infrared (FTIR) spectroscopy also confirmed the existence of SO_4^{2-} (**Figure S4**), which may be introduced into DTD-Cu by forming H-bond with -NH_2 of DTD.[21] Importantly, the appearance of Cu-S implied that apart from two N atoms, the thiophenic S of DTD could also coordinated with Cu ion. These XPS and TOF-SIMS spectra corporately illustrated that DTD-Cu involved the Cu-N and Cu-S coordination centers.

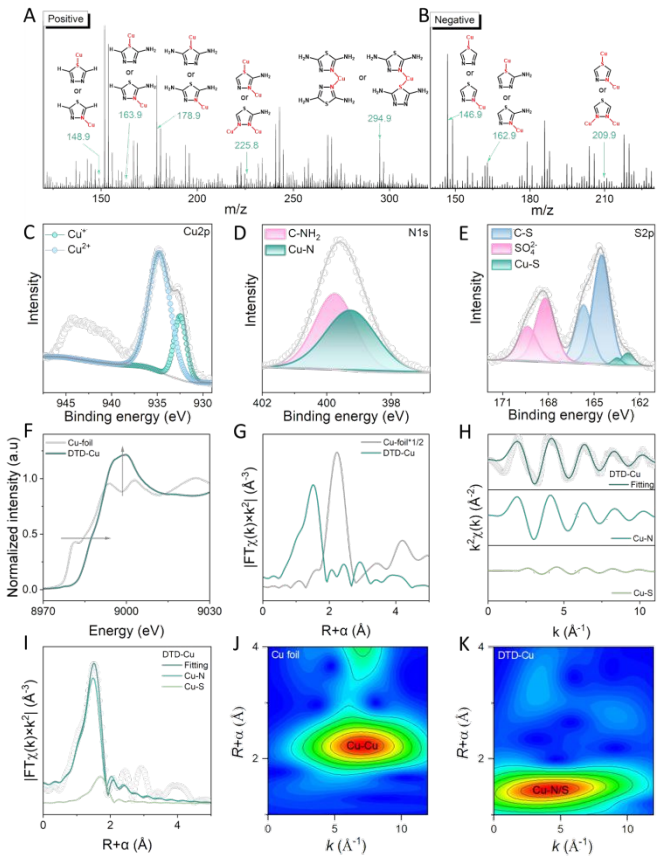

Figure 2 TOF-SIMS spectra of positive (A) and negative (B) ions and possible assignments; Cu2p (C), N1s (D) and S2p (E) XPS spectra of DTD-Cu; (F) Cu K-edge XANES spectra of DTD-Cu and Cu foil; (G) Cu K-edge FT-EXAFS spectra of DTD-Cu and Cu foil in R space; (H) Cu K-edge EXAFS fitting analysis of DTD-Cu in k-space; (I) FT-EXAFS fitting analysis of DTD-Cu in R-space. Cu K-edge WT-EXAFS spectra of Cu foil (J) and DTD-Cu (K).

X-ray absorption near-edge structure (XANES) spectroscopy and extended X-ray absorption fine structure (EXAFS) was further analyzed to determine the atomic-scale coordination

View Article Online
DOI: 10.1039/D5SC05473A

information of Cu in DTD-Cu. As shown in Cu K-edge X-ray absorption near-edge structure (XANES) spectroscopy, the edge absorption energy of DTD-Cu was more positive than that of Cu foil (**Figure 2F**). Moreover, DTD-Cu also exhibited the higher intensity of white line peak corresponding to the 1s → $4p_{xy}$ transition compared with Cu foil. These results indicated that the Cu center of DTD-Cu was in the oxidation state.

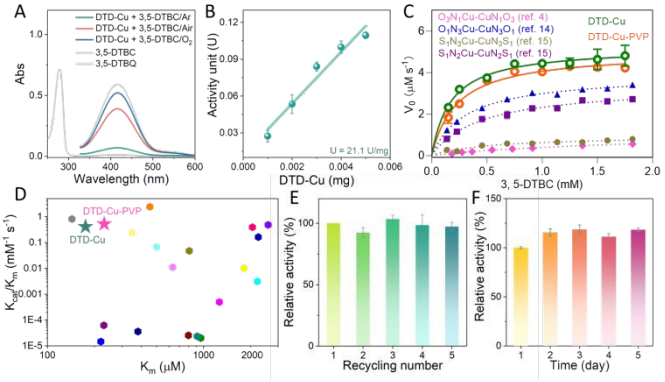

Figure 3 (A) UV–vis spectra of 3,5-DTBC, 3,5-DTBQ as well as 3,5-DTBC in air-, O_2- and N_2-saturated PBS (pH=8)/CH_3CN solution with DTD-Cu; (B) Specific activity of DTD-Cu; (C) Michaelis–Menten curves of DTD-Cu and recently reported nanozymes; (D) Comparison of kinetic parameters (K_m and K_{cat}/K_m) among DTD-Cu, recently reported artificial molecular enzymes and nanozymes; (E) Relative activities of DTD-Cu during recycling process; (F) Storage stability of DTD-Cu in air at room temperature.

Fourier-transformed EXAFS spectrum (FT-EXAFS) in R space displayed that DTD-Cu showed the characteristic scattering peak at ~ 1.50 Å, obviously distinct from the Cu-Cu scattering peak at ~ 2.24 Å (**Figure 2G**), suggesting the atomic dispersion of Cu in DTD-Cu. According to FT-EXAFS signal in k-space, we observed two different oscillation periods corresponding to Cu-N and Cu-S paths (**Figure 2H**), which favored the formation of Cu-N and Cu-S coordination in DTD-Cu, agreeing with the N1s/S2p spectra (**Figure 2D** and **2E**). To determine the N/S coordination numbers around the Cu center, the fitting analysis of FT-EXAFS spectrum of DTD-Cu in R space was performed. **Figure 2I** and **Table S1** illustrated that each Cu center was connected with four N atoms, and the average number of coordinating S atom was 0.5 in DTD-Cu, which reflected that only one Cu atom of the adjacent dicopper centers coordinated with the thiophenic S atom of DTD, thus generating the asymmetric N_4Cu-CuN_4S configuration at the adjacent dicopper centers. In addition, the intensity maximum of wavelet-transformed (WT)-EXAFS spectra of DTD-Cu situated at ~1.46 Å, which were clearly different from that of Cu foil (2.23 Å). This verified the atomic disperse of Cu in DTD-Cu, consistent well with FT-EXAFS. All of these results illustrated that the N/S-rich DTD ligand was prone to coordinate with Cu through the Cu-N and Cu-S bonds, accompanied with generating the asymmetric N_4Cu-CuN_4S configuration at the adjacent binuclear Cu centers of DTD-Cu.

Using 3,5-ditert-butyl catechol (3,5-DTBC) as a model molecule, we evaluated the catechol oxidase-like catalytic activity of DTD-Cu. As depicted in **Figure 3A**, the characteristic absorbance of 3,5-DTBC in the air-saturated blank solution was situated at 280nm. After DTD-Cu was mixed with 3,5-DTBC in the catalytic system, the colorless solution gradually became yellow and the new peak at 416nm occurred, which was assigned to the product 3,5-ditert-butyl-benzoquinone (3,5-DTBQ). This demonstrated the catechol oxidase-like activity of DTD-Cu. Moreover, increasing the O_2 concentration of the catalytic system led to the obvious enhancement of the catalytic activity of DTD-Cu, suggesting that DTD-Cu was capable to activate O_2 to oxidize 3,5-DTBC. Once DTD-Cu was filtered by a filter membrane with average pore size of 100 nm, the reaction rate obviously decreased (**Figure S5**). When the pH of the buffer solution varied from 3 to 8, DTD-Cu presented the enhanced catalytic activity (**Figure S6**). In order to compare with the reported catechol oxidase-like artificial enzymes,[1, 4] the buffer solution with the pH of 8 was chose to assess the catalytic activity of DTD-Cu. Meanwhile, the catalytic activity of DTD-Cu did not notably decrease after adding K^+, Na^+ and Cl^- into the catalytic system (**Figure S7**).

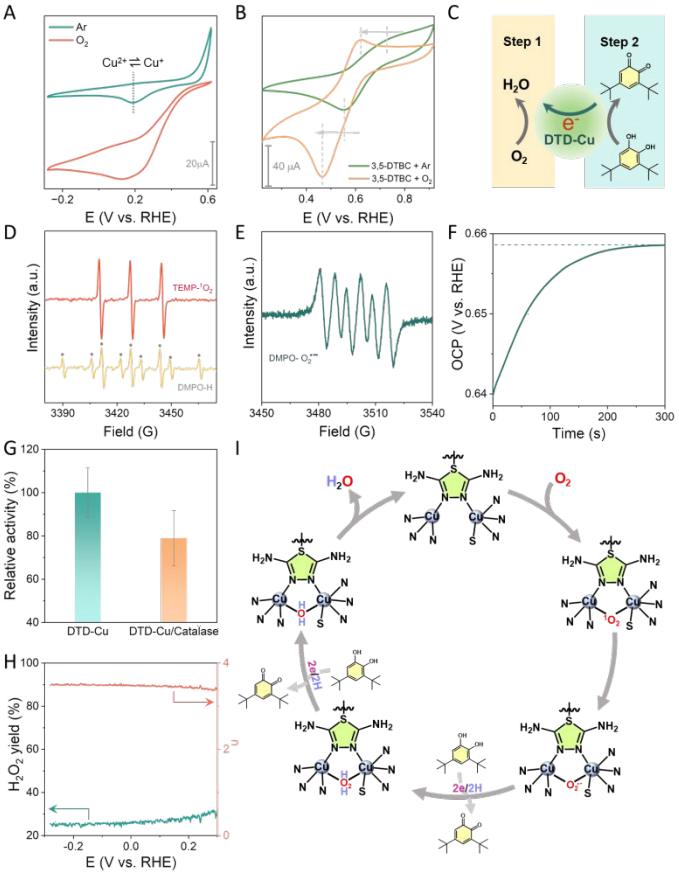

Figure 4 (A) CV curves of DTD-Cu in the presence of Ar or O_2; (B) CV curves of DTD-Cu in presence of 3,5-DTBC as well as Ar or O_2; (C) Schematic illustration of electron transfer in the processes of 3,5-DTBC oxidation and O_2 reduction; ESR spectra recorded for trapping $^1O_2$/$^•$OH (D) and $O_2^{•-}$ (E); (F) OCP curve over time; (G) Specifically trapping H_2O_2 during DTD-Cu-catalyzed oxidation of 3,5-DTBC using catalase; (H) Electron transfer number (n) and H_2O_2 yield of DTD-Cu during electrocatalytic oxygen reduction; (I) Proposed mechanism of mimicking CO-like catalysis at dicopper sites of DTD-Cu.

According to **Figure 3B**, the specific activity of DTD-Cu approached to 21.1U/mg. Moreover, DTD-Cu-PVP with the smaller size showed the higher specific activity, which reached 38.6 U/mg (**Figure S8**), superior to many reported catechol oxidase-like artificial enzymes (**Table S2**).[13-15] Meanwhile, the

View Article Online
DOI: 10.1039/D5SC05472A

intrinsic activity of DTD-Cu was further evaluated by changing the concentration of 3,5-DTBC. The catalytic reaction rate shown by DTD-Cu followed Michaelis–Menten kinetics (**Figure 3C**) and surpassed the reported nanozymes with the symmetric dicopper site configurations (i.e., S_1N_3Cu-CuN_3S_1, S_1N_2Cu-CuN_2S_1, O_1N_3Cu-CuN_3O_1, O_3N_1Cu-CuN_1O_3).[4, 14, 15] Based on the Michaelis–Menten equation, the kinetic parameters involving K_m, K_{cat} and K_{cat}/K_m were further acquired by non-linear curve fitting analysis. As seen in **Figure 3D and Table S3**, the K_m and K_{cat}/K_m values of DTD-Cu exceeded most catechol oxidase-like artificial enzymes and nanozymes,[1, 4, 5, 12, 14, 15, 19, 22] demonstrating the superior catalytic activity of DTD-Cu. The relative activity of DTD-Cu did not decrease after five recycling (**Figure 3E**). Even after being stored in water for 5 days, DTD-Cu did not show the significant decay of catalytic activity (**Figure 3F**). These activity assessments demonstrated the superior catalytic capability of DTD-Cu, which was promising to act as a new artificial enzyme for the catalytic colorimetric detection.

To further understand the catalytic mechanism of DTD-Cu, the electrochemical characterization, EPR testing and specific capture experiment were performed, respectively. In the Ar-saturated solution with the pH of 8, the redox transition peak of Cu^{2+}/Cu^{+} was presented in the cyclic voltammetry (CV) curve of DTD-Cu. After this solution was saturated by O_2, a strong reduction current was observed (**Figure 4A**), indicating the obvious oxygen reduction activity of DTD-Cu. Importantly**,** we also found the obvious redox peaks in the CV curves of **Figure 4B** when DTD-Cu catalyzed the 3,5-DTBC oxidation. However, once Ar was replaced by O_2, these redox peaks shifted negatively. This may be due to that O_2 was easier to be preferentially adsorbed and activated at the binuclear Cu sites of DTD-Cu during catalysis compared with 3,5-DTBC (**Figure 4C**), which led to the elevated electrochemical potential, making the oxidation of 3,5-DTBC become easier. The collected electron spin resonance (ESR) spectra supported this deduction, which showed that the obvious $^1O_2$ signal was detected for DTD-Cu only in the presence of air and TEMP without adding 3,5-DBTC (**Figure 4D**). Due to the asymmetric configuration of dicopper centers, the O-O bond in the formed $^1O_2$ could be further polarized by acquiring electron from the Cu site to produce $O_2^{\bullet-}$ only in the presence of air and DMPO without adding 3,5-DBTC (**Figure 4E**).

Once the Cu sites transferred electron to polarize the adsorbed O_2 to form $O_2^{\bullet-}$, DTD-Cu became more electron-deficient, thus elevating the electrochemical potential of DTD-Cu to drive the 3,5-DBTC oxidation. Meanwhile, this rising electrochemical potential endowed DTD-Cu with a worse reducing capability, which would attenuate the rate of oxygen reduction reaction (ORR). Accordingly, the "mixed potential" (i.e., open-circuit potential (OCP)) of reductive and oxidative half-reactions[14, 23] would experience a continuous change until the rates of ORR and oxidation of 3,5-DBTC were balanced to attain a steady state, which could be supported by the collected OCP curve (**Figure 4F**). These results confirmed that the preferential adsorption and activation of O_2 was the crucial initial step during mimicking CO-like catalysis, and the asymmetric dicopper centers of DTD-Cu subsequently polarized the O-O bond to generate $O_2^{\bullet-}$ by transferring electron.

The formed $O_2^{\bullet-}$ further acquired electrons and protons to produce H_2O_2, which was demonstrated through the catalase trapping experiment (**Figure 4G**). This H_2O_2 intermediate was also detected by the rotating ring-disc electrode (RRDE) test (**Figure 4H**). Given that the ORR driven by DTD-Cu belonged to a 4e-dominated process (**Figure 4H**), the produced H_2O_2 could be further reduced to form H_2O by accepting electrons and protons, accompanied with the oxidation of 3,5-DTBC. Interestingly, the $^{\bullet}OH$ signal was not detected during catalysis. Thus, the possible catalytic mechanism driven by DTD-Cu was proposed (**Figure 4I**). After O_2 was preferentially adsorbed at the Cu site of DTD-Cu, it experienced the continuous 4e transformation process of $^3O_2 \rightarrow {}^1O_2 \rightarrow O_2^{\bullet-} \rightarrow H_2O_2 \rightarrow H_2O$, which was accompanied with the oxidation of 3,5-DTBC.

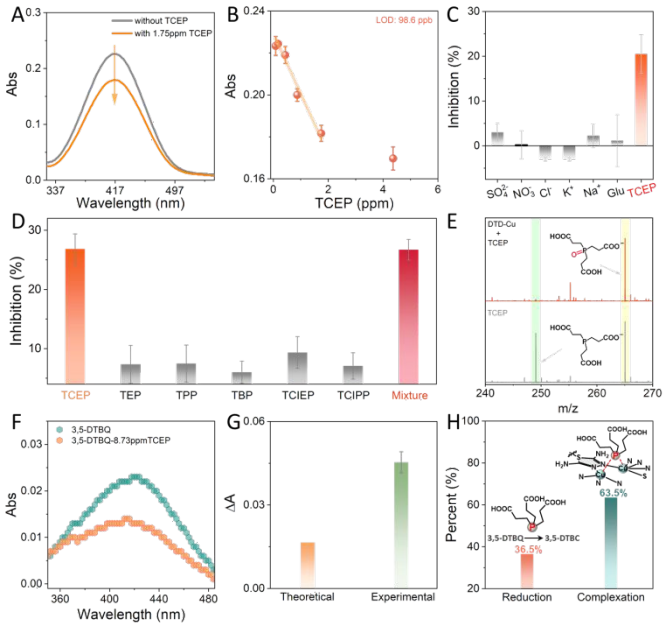

Figure 5 (A) UV–vis spectra of monitoring the DTD-Cu-catalyzed 3,5-DTBC oxidation in the absence and presence of TCEP; (B) Linear plot of absorbance (416nm) versus the concentration of TCEP in the DTD-Cu-driven colorimetric system; Selectivity of DTD-Cu for detecting TCEP in the presence of various interfering ions (C) and organophosphorus molecules (D); (E) High-resolution mass spectrometry of reaction solution involving DTD-Cu and TCEP; (F) UV–vis spectra of 3,5-DTBQ in the absence and presence of TCEP; (G) Comparison of theoretical and experimental absorbance of systems in the presence of 1.75ppm TCEP; (H) Contribution of reduction and complexation originating from TCEP on inhibiting catalytic colorimetric process of DTD-Cu.

Based on this catalytic colorimetric system enabled by the outstanding CO-like catalytic activity of DTD-Cu, we detected organophosphorus compounds that were usually involved in flame retardants, pesticides and insecticides.[24, 25] We chose cytotoxic tris(2-carboxyethyl)phosphine (TCEP) as a model P-based compound.[26] TCEP was directly mixed with the reaction solution involving DTD-Cu and 3,5-DTBC. After 3min, the solution was monitored using the UV-vis spectroscopy. Compared with the control group, the absorbance of solution decreased significantly once 1.75ppm TCEP was introduced (**Figure 5A**), indicating this catalytic colorimetric system driven by DTD-Cu was available for detecting TCEP. By varying the

View Article Online
DOI: 10.1039/D5SC05473A

concentration of TCEP in the catalytic system, the limit of detection (LOD) was determined to be 98.6ppb (**Figure 5B**), which was comparable to other sensing systems for detecting organophosphorus compounds based nanozymes, surface-enhanced Raman spectroscopy (SERS) and fluorescence (**Table S4**).[27-29] Furthermore, the LOD for sensing TCEP in this DTD-Cu system was also lower than the methods of HPLC-ELSD and other nanozyme catalytic system (**Table S4**). Importantly, apart from TCEP, various inorganic ions (K^+, Na^+, Cl^-, NO_3^-, SO_4^{2-}), glucose (Glu) and phosphate ester flame retardants such as triethyl phosphate (TEP), triphenyl phosphate (TPP), tributyl phosphate (TBP), tris (2-chloroethyl) phosphate (TClEP) and tris(1-chloro-2-propyl) phosphate (TClPP) did not show the notable inhibition effect on the DTD-Cu-driven catalytic colorimetric system (**Figure 5C** and **5D**). According the reported result,[30] the molecular volume of TPP and TCEP was similar, indicating their similar steric effects. However, the inhibition effect of TPP on the catalytic activity of DTD-Cu was much poorer (**Figure 5D**). Such a result indicated that the steric effect was not the main reason for the selective sensing behavior of DTD-Cu for these organophosphorus compounds. Likewise, the catalytic activity of DTD-Cu did not present the notable decrease after adding the reducing epinephrine into this catalytic system, which was different from the phenomenon of adding TCEP (**Figure S9**). This indicated that TCEP could be selectively detected using this DTD-Cu-driven catalytic system.

Given that DTD-Cu activated O_2 to generate ROS during catalysis and TCEP was capable to quench ROS, we speculated that TCEP may inhibit the catalytic colorimetric process by quenching ROS. If this deduction was reasonable, the oxidation product of TCEP could be detected. To verify the above deduction, high-resolution mass spectrometry (HRMS) was conducted to analyze the reaction solution containing DTD-Cu and TCEP. The oxidation product tris(carboxyethyl)phosphine oxide (TCEPO) was found, and TCEP almost disappeared after 3min (**Figure 5E**). Such a result illustrated that ROS may be quenched by the electron-rich P of TCEP through the reduction reaction. Moreover, individually adding TCEP to the yellow 3,5-DTBQ solution without DTD-Cu made the absorbance of solution obviously decreased (**Figure 5F**), which was due to that TCEP was capable to reduce 3,5-DTBQ.[31]

Both quenching ROS and reducing 3,5-DTBQ would essentially cause the oxidation of TCEP to form TCEPO, which was accompanied with the 2e transfer. Consuming one TCEP molecule was equivalent to eliminating one 3,5-DTBQ molecule. If we assumed that TCEP inhibited the catalytic colorimetric process only by quenching ROS and reducing 3,5-DTBQ, the absorbance change of solution was theoretically calculated based on the linear working curve of 3,5-DTBQ. According to this assumption, the theoretical absorbance change of solution should be 0.017 once adding 1.75 ppm TCEP (**Figure 5G**). However, the experimental result showed that the absorbance change of solution was 0.045, significantly exceeding the theoretical value. Such a result, together with the coordination potential of electron-rich P in the TCEP, illustrated that in addition to quenching ROS and reducing 3,5-DTBQ, TCEP was capable to compete with O_2 for the Cu sites of DTD-Cu via the complexation effect to inhibit the catalytic colorimetric process.[32] Accordingly, we calculated that the inhibition originated from the complexation effect and reduction potential of TCEP accounted for 63.5% and 36.5%, respectively (**Figure 5H**), which suggested that the contribution of the complexation effect on inhibiting the catalytic colorimetric process was dominant compared with that of quenching ROS and reducing 3,5-DTBQ, thereby enabling the selective detection of TCEP using this DTD-Cu-driven catalytic colorimetric system.

Conclusions

In summary, we have addressed the challenge of low intrinsic activity in CO-mimicking nanozymes by designing the proximal and asymmetrically coordinated dicopper catalytic centers in DTD-Cu. This unique ligand-mediated asymmetric N_4Cu-CuN_4S configuration enabled a dramatic enhancement in CO-like catalytic efficiency by orders of magnitude compared to previously reported nanozymes and artificial enzymes. Leveraging this exceptional catalytic performance as well as the high affinity of Cu for phosphorus, we developed a highly selective and sensitive colorimetric sensing platform for TCEP, achieving a detection limit of 98.6 ppb. This outstanding sensing capability was attributed to a synergistic dual-inhibition mechanism involving both TCEP-induced reduction of the oxidized substrate and direct TCEP chelation to the copper active sites, with the latter playing a dominant role in achieving high selectivity. This work not only presented a breakthrough in designing highly active biomimetic dicopper nanozymes by precisely tuning ligand-mediated asymmetry but also offered a powerful platform for catalytic sensing, opening new avenues for advanced catalyst design.

Author contributions

F. H. conceived and designed the experiments. B. L. performed the synthesis and/or activity evaluation of nanozyme. N. X. provided help for applying for the founding. F. H. wrote and revised the manuscript. F. H. and X. H. supervised the project.

Conflicts of interest

The authors declare no competing financial interests.

Data availability

The data that supports the findings of this study is available from Supporting Information.

Acknowledgements

This work was financially supported by National Natural Science Foundation of China (No. 52276195), Doctoral Fund Project of University of Jinan (XBS2409), Opening Project of State Key Laboratory Incubation Base for Green Processing of Chemical

Engineering (Shihezi University, China), the Foundation (No. GZKF202335) of State Key Laboratory of Biobased Material and Green Papermaking (Qilu University of Technology, Shandong Academy of Sciences), Program for supporting innovative research from Jinan (202228072) and Program of agricultural development from Shandong (SD2019NJ015). The authors extend their gratitude to Mr. Yanda Du from Shiyanjia Lab (https://www.shiyanjia.com) for providing invaluable assistance with the XPS analysis.

Notes and references

1. M. Li, J. Chen, W. Wu, Y. Fang and S. Dong, *J. Am. Chem. Soc.*, 2020, **142**, 15569-15574.
2. S. Ji, B. Jiang, H. Hao, Y. Chen, J. Dong, Y. Mao, Z. Zhang, R. Gao, W. Chen and R. Zhang, *Nat. Catal.* 2021, **4**, 407-417.
3. P. Makam, S. S. Yamijala, V. S. Bhadram, L. J. Shimon, B. M. Wong and E. Gazit, *Nat. Commun.*, 2022, **13**, 1505.
4. M. Sha, L. Rao, W. Xu, Y. Qin, R. Su, Y. Wu, Q. Fang, H. Wang, X. Cui and L. Zheng, *Nano Lett.*, 2023, **23**, 701-709.
5. S. Xu, H. Wu, S. Liu, P. Du, H. Wang, H. Yang, W. Xu, S. Chen, L. Song and J. Li, *Nat. Commun.*, 2023, **14**, 4040.
6. Y. Xu, J. Xue, Q. Zhou, Y. Zheng, X. Chen, S. Liu, Y. Shen and Y. Zhang, *Angew. Chem. Int. Ed.*, 2020, **59**, 14498-14503.
7. G. Li, H. Liu, T. Hu, F. Pu, J. Ren and X. Qu, *J. Am. Chem. Soc.*, 2023, **145**, 16835-16842.
8. J. Wang, R. Huang, W. Qi, R. Su, B. P. Binks and Z. He, *Appl. Catal. B Environ.*, 2019, **254**, 452-462.
9. Y. Lin, F. Wang, J. Yu, X. Zhang and G.-P. Lu, *J. Hazard. Mater.*, 2022, **425**, 127763.
10. W. Zou, Y. Liu, R. Li and R. Guo, *ACS Sustain. Chem. Eng.*, 2022, **10**, 10057-10067.
11. D. Kim, G. Gwak, J. Han, D. Kim and O. S. Jung, *Dalton Trans.*, 2022, **51**, 5810-5817.
12. J. Wang, R. Huang, W. Qi, R. Su and Z. He, *Chem. Eng. J.*, 2022, **434**, 134677.
13. M. Yuan, K. Han, H. Yang, L. Mi, C. Huang, X. Hu and F. He, *Small*, 2024, e2401756.
14. M. Yuan, N. Xia, X. Hu and F. He, *Small*, 2024, **20**, e2403850.
15. M. Yuan, N. Xia, Z. Huang, C. Huang, X. Hu and F. He, *Chem Sci*, 2024, **15**, 19513-19519.
16. R. V. Morajkar, A. P. Fatrekar and A. A. Vernekar, *Chem Sci*, 2024, **15**, 10810-10822.
17. T. Klabunde, C. Eicken, J. C. Sacchettini and B. Krebs, *Nat. Struct. Biol.*, 1998, **5**, 1084-1090.
18. C. Gerdemann, C. Eicken and B. Krebs, *Acc. Chem. Res.*, 2002, **35**, 183-191.
19. S. Thanneeru, N. Milazzo, A. Lopes, Z. Wei, A. M. Angeles-Boza and J. He, *J. Am. Chem. Soc.*, 2019, **141**, 4252-4256.
20. Y. X. Zhang, S. Zhang, H. Huang, X. Liu, B. Li, Y. Lee, X. Wang, Y. Bai, M. Sun, Y. Wu, S. Gong, X. Liu, Z. Zhuang, T. Tan and Z. Niu, *J. Am. Chem. Soc.*, 2023, **145**, 4819-4827.
21. E. Aznar, S. Ferrer, J. Borrás, F. Lloret, M. Liu‐González, H. Rodríguez‐Prieto and S. García‐Granda, *Eur. J. Inorg. Chem.*, 2006, **2006**, 5115-5125.
22. S. Liu, Y. He, W. Zhang, T. Fu, L. Wang, Y. Zhang, Y. Xu, H. Sun and H. Zhao, *Small*, 2024, **20**, e2306522.
23. W. C. Howland, J. B. Gerken, S. S. Stahl and Y. Surendranath, *J. Am. Chem. Soc.*, 2022, **144**, 11253-11262.
24. X. Wang, S. Dong, Q. Zhu, X. Wu, W. Zhou, C. Liao and G. Jiang, *Environ. Sci. Technol.*, 2024, **58**, 14786-14796.
25. B. Shen, Q. Wu, Y. Guo, J. Qin, H. Chen, Y. Yang, Z. Liu, L. Li, W. Li and C. Zhu, *Adv. Funct. Mater.*, 2024, **35**, View Article Online DOI: 10.1039/D5SC05472A
26. I. Koh, I. Yong, B. Kim, D. Choi, J. Hong, Y. M. Han and P. Kim, *ACS Biomater. Sci. Eng.*, 2020, **6**, 813-821.
27. X. Yan, H. Li, Y. Yan and X. Su, *Food Chem.*, 2015, **173**, 179-184.
28. J. Sun, L. Gong, Y. Lu, D. Wang, Z. Gong and M. Fan, *Analyst*, 2018, **143**, 2689-2695.
29. P. Weerathunge, B. K. Behera, S. Zihara, M. Singh, S. N. Prasad, S. Hashmi, P. R. D. Mariathomas, V. Bansal and R. Ramanathan, *Anal. Chim. Acta*, 2019, **1083**, 157-165.
30. B. Li, N. Xia, C. Huang, X. Hu and F. He, *Chem Sci*, 2025, **16**, 14793-14799.
31. B. C. Martindale, E. Joliat, C. Bachmann, R. Alberto and E. Reisner, *Angew. Chem. Int. Ed.*, 2016, **55**, 9402-9406.
32. P. Mei, Z. Ma, Y. Chen, Y. Wu, W. Hao, Q.-H. Fan and W.-X. Zhang, *Chem. Soc. Rev.*, 2024, **53**, 6735-6778.

View Article Online
DOI: 10.1039/D5SC05472A

Data Availability Statement

The data that supports the findings of this study is available from Supporting Information.